Energetic Electron Injection and Precipitation as Seen from RCM Bubble Simulation

Victor Sergeev, **Jian Yang**, **Weiqin Sun**, **and Maria Shukhtina**

Abstract Although principal possibility to form the energetic electron (EE) injections by transient fast flow bursts was demonstrated, details and quantitative aspects of injection process need to be further investigated based on advanced models. Here we use self-consistent RCM-I simulation initiated by the short-duration (5-min long) localized (~3 Re width) density depletion (evacuating 90% of flux tube content) at the tailward simulation boundary (~18 Re) to look on resulted dynamics of energetic electrons as they are accelerated, injected and then drift eastward in the magnetosphere and precipitate into the atmosphere. We demonstrate that, starting from ordinary plasma sheet population, 50–200 keV electron flux dramatically increases by betatron-like acceleration when the bubble head enter the inner magnetosphere at r < 8–10 Re, and finally reaches as high flux values as 10^5 $(cm^2\ s\ sr\ keV)^{-1}$ forming an injected electron cloud. At this time, a sudden onset of EE precipitation develops in the conjugate ionosphere in a couple of minutes. Although simulation uses some approximations (like isotropic precipitation from drifting cloud) and describes an elementary act of injection, it is capable to reproduce basic known global features of precipitation dynamics and geometry including eastward drift along the auroral zone (with roughly 1 h drift period) and a crescent-shaped precipitation zone with minimal precipitation at dusk.

Keywords Bursty bulk flows · Energetic electron injection · Energetic electron precipitation

V. Sergeev (✉) · M. Shukhtina
St. Petersburg State University, St. Petersburg 198504, Russia
e-mail: victor40sergeev@gmail.com

J. Yang · W. Sun
Southern University of Science and Technology, Shenzhen 518055, China

1   Introduction

Sudden large increases of energetic electron (EE, here 30–300 keV) fluxes, often referred to as the EE injections, are known since first spacecraft observations made at geostationary orbit. It was soon established, that near midnight these flux enhancements are observed simultaneously at all energies together with bay-like increases of magnetic field H (Bz) component, called magnetic dipolarization [1]; these observations were attributed to the rapid earthward injection of plasma tubes during substorms. Outside of this azimuthally localized injection region, at other local times, the registered energy-dependent arrivals of EE flux increases were interpreted as the eastward magnetic drift of EE cloud injected near midnight. Large increases of magnetospheric EE flux are accompanied by intense EE precipitation in magnetically conjugate regions of auroral ionosphere [2]. Both these phenomena are now recognized as significant Space Weather threats because of their influence on the operation of spacecraft instruments/systems, on radio-communications etc.; the EE precipitation also modifies the atmosphere, providing long-term influence on ozon and climate [3].

Whereas the magnetospheric origin and abovementioned general view of EE injections are widely recognized, their important physics details are not fully established yet. Observationally there exist a bulk of evidence connecting the injections to the sporadic and localized fast earthward flows in the magnetotail plasma sheet (BBFs, [4]), see a summary in [5]. BBFs are inherently the plasma bubbles (possess the reduced density, thermal pressure P and plasma tube entropy $PV^{5/3}$, where V is the volume of unit magnetic flux plasma tube); this property helps them to penetrate into the dipole-like inner magnetosphere [6, 7]; the bubble origin is intimately connected to the low density of plasma tubes participating in the sporadic activations of localized magnetic reconnection in the magnetotail [8].

There are little doubts that betatron-like acceleration plays an important role in providing large energetic particle fluxes [8], but details of its realization are important and they differ between different models. The particle trajectories are complicated and highly variable depending on particle energy and pitch-angle, this is why most studies used test particle approach using predetermined (analytical or MHD-simulated) electromagnetic fields. Whereas in some simulations energetic particles transported to the geosynchronous distance entered through the flanks of the fast flow channel and have limited transportation distance of few Re (e.g. [8, 9], other simulations showed possibility of long pathway of >10 Re with energetic particles captured within fast flow channels [5, 10] A number of effects, which assist in extended capture of energetic particles inside the flows and their more efficient acceleration, include magnetic drift at the dipolarization front and at flanks of the dipolarized flow channel, they were recently summarized in [5].

Although the abovementioned studies agree in qualitative sense that fast plasma flows are capable to accelerate and transport energetic electrons into the inner magnetosphere, diversity of models and non-self-consistent realization and not fully realistic setup (in setting plasma and magnetic configuration, including dipole-like field) make

it difficult to get realistic quantitative description. The requirements for such model are that it should be the high-resolution 3-D model, which treating self-consistently the coupling between ionosphere and magnetosphere and dynamic plasma/B interactions, and also include particles of different energies taking into account their magnetic and ExB drifts. Also, the abovementioned papers were focused mainly on the acceleration and injection aspects without considering self-consistently the following destiny of injecting particles.

Our study aims on providing quantitative assessment of acceleration and details of global development of injected, drifting and precipitating EE cloud based on advanced version of RCM model. Here we focus on describing:–how/where the EE cloud grows and releases;–how/where the EE cloud inner boundary is formed, and–what is the global dynamics and flux variation of electrons injected into the inner magnetosphere and precipitated into the ionosphere during the subsequent drift of electron cloud.

2 Simulation Results

2.1 Simulation Setup

Generic bubble injection is simulated using recent version of the Rice Convection Model (RCM, [11]) two-way coupled with an 3d MHD code [12]. Both $E \times B$ and gradient/curvature drifts are calculated for proton and electron isotropic subpopulations, each distributed in 220 energy invariant channels. Here we use a high grid resolution, with 0.03° in latitude and 1.3° in longitude in the auroral zone; being mapped in the near-Earth plasma sheet, this corresponds approximately to 0.05 and 0.1 R_E in the X and Y directions. Initial and boundary conditions are set up similar to our previous simulations [13] based on empirical models; electric potential drop across the simulation region is kept to be 46 kV. For the first hour of the run, we simulate a substorm-growth-phase-like quasi-steady convection, without bubble injections. At T = 60 min, we initiate the bubble at tailward boundary (r ~ 18 Re) by decreasing the density and flux-tube entropy $PV^{5/3}$ (in 1 min) to 10% of their pre-injection values in the region between 23.5 and 0.5 h in local time (as shown in panel **a1** in Fig. 1). They kept constant until T = 66 min, when in one minute both density and $PV^{5/3}$ increase to their pre-injection values, at which the boundary parameters are held until the end of simulation run (T = 120 min).

After being launched from tailward boundary (column **a** in Fig. 1) the bubble developed earthward: in 3 min it reached 12 Re (at 64 min, column **b**) and at 67 min (column **c**) its front intruded up to 7Re, passing inside the geostationary orbit during a couple of minutes. The blue bubble and associated convection enhancements are seen most distinct in the entropy plots (row 1). Bz plots in row 2 demonstrate dipolarized magnetic field inside of and propagating with the bubble. Third row shows the distribution of 50–75 keV electron flux which is of main interest to us. Before
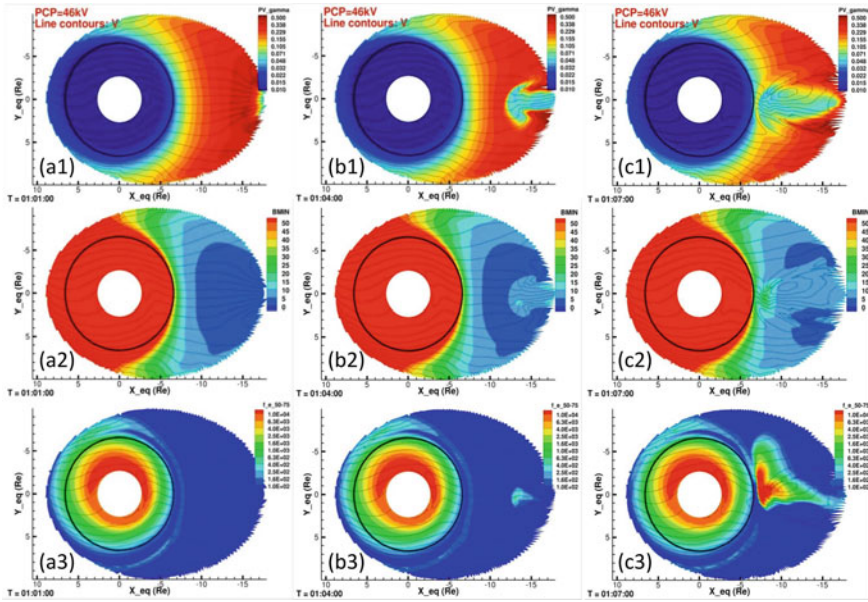
Fig. 1 Equatorial distribution of parameters during the bubble initiation (column **a**), its propagation in the plasma sheet (column **b**) and flow braking in the inner magnetosphere (column **c**). Rows from top to the bottom show distributions of plasma tube entropy (PV$^{5/3}$), magnetic field (Bz) and differential flux of 50–75 keV electrons. Electric potential lines are also shown; black circles indicate the geostationary orbit

and at the bubble initiation (**a3** in Fig. 1) there were no significant EE fluxes in the tail except for the radiation belt prescribed in the inner magnetosphere at the initial state. Some signatures of enhanced electrons are visible within the bubble during its propagation in the plasma sheet (**b3**) but the fluxes are rather weak, they increased substantially only during the flow braking stage when the bubble approached close to the geostationary orbit and particles drift out from the acceleration site (**c3**).

2.2 Energetic Electron Acceleration Associated with the Bubble Development

To look into the bubble braking stage and acceleration-related issues in more details, we plot in Fig. 2 the radial profiles of important parameters along the axis of fast flow.

The right-hand side plots show the radial variations of major parameters at the epoch of maximal EE fluxes and their closest approach to Earth, i.e. the injection peak (T = 68 min). It allows to relate EE flux variations to the bubble structure
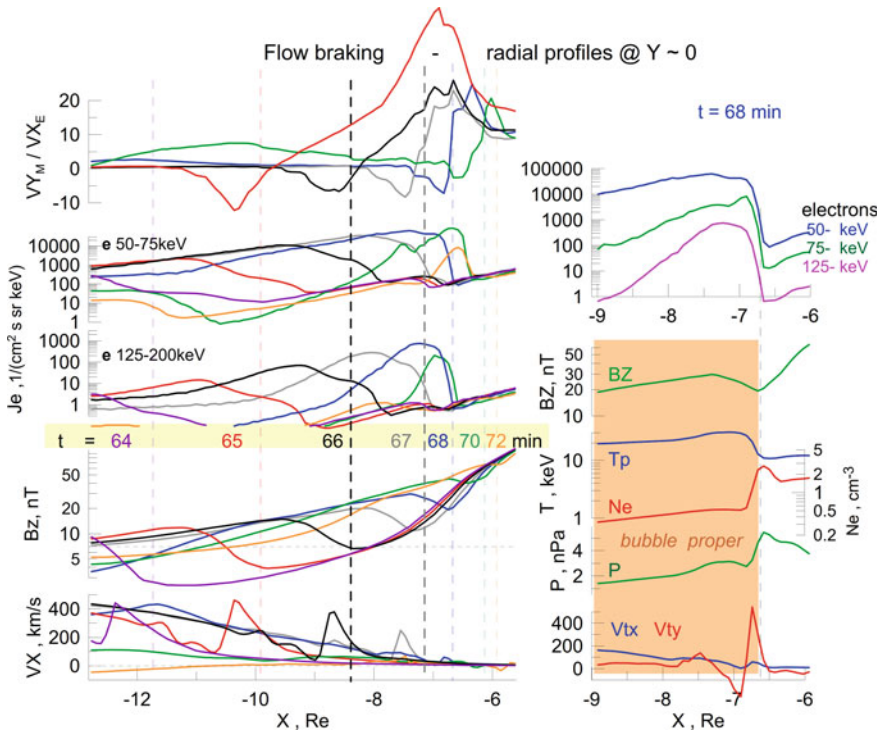
Fig. 2 Radial profiles of parameters along the axis of fast flow channel. The right-hand-side plots show the radial variations of major parameters at the epoch of maximal EE fluxes and their closest approach to Earth (T = 68 min). Shaded area indicates the bubble proper. The left-hand plots characterize a time progression of radial profiles as the bubble intrudes into the inner magnetosphere. The upper plot shows the ratio of azimuthal magnetic drift velocity (VY_M, for 50 keV energy) to the earthward convection flow in the bubble (VX_E). Colored vertical dashed lines denote the bubble front locations

(shaded area), which is characterized by the depression of plasma density and pressure, increase of equatorial magnetic field and plasma temperature, and enhanced plasma flow (Vtx). The fluxes of energetic electrons are clearly enhanced within the bubble, they have a common inner boundary and their profile nearly corresponds to the Bz profile in the bubble. The left-hand plots characterize a progression of radial profiles as the bubble intrudes into the inner magnetosphere. Its braking is manifested by decreasing velocity of bubble front and plasma flow speed (VX) as the bubble intrudes inward.

There are few things to note from these plots. The peak magnetic field progressively increases from 10–15 nT in the plasma sheet (at > 10 Re) to > 30 nT where the peak fluxes are observed, and EE fluxes follow these changes in both 50- and 125-keV energy channels. The ratio of azimuthal magnetic gradient drift speed (VY_M) to the earthward convective flow (VX_E) shown in the upper left plot is of vital importance.

Here we see the region of negative (westward) VY_M in the area of Bz dipolarization front where energetic electrons are deflected westward while they stay in the DF region (known as a surfing region according to [9]. We notice that transition from westward to (normal) eastward direction of electron drift nearly corresponds to the termination of EE flux in the bubble front. Thickness of this transition region shrinks with the time, and the sharpest gradients of both magnetic field and VY_M are observed at $T = 68$ min where/when sharp inner flux boundary is observed in all EE channels plotted in the left upper plot of Fig. 2.

To characterize the energy gain in the flow channel and its progression with time we plotted in Fig. 3 the profile of particle fluxes J against B along the X-axis, which starts from 14Re distance and ends at the distance where the magnetic field attained its peak in the flow channel. For 50 keV electrons (Fig. 3a) the colored traces at 65, 66, 67 min are closely grouped together, this occurs in the region where the actual particle trajectories are mostly determined by fast convective flow in the narrow stream. In this case the grouped traces characterize the efficiency of betatron acceleration and the tenfold peak flux increase between 65 and 67 min is related to the nearly twofold increase of peak B value in the braking bubble while it propagated into the strong magnetic field of the inner magnetosphere. The blue profile at 68 min is similar in its upper part, but deviate from this behavior at 12–14 Re because the information about switch-off of the bubble (at 66 min) propagated to that distance. The decline of fast flows over most of the region drastically changed the trajectories and terminated the acceleration, this is why J(B) profile at 70 min is highly different from previous ones. For 125 keV electrons, profiles at 65 and 66 min are also grouped, but acceleration terminated earlier (since 67 min).

As follows from Figs. 2 and 3, the peak fluxes are reached at 68/70 min, at later time further acceleration fails because the fast flow channel is destroyed. The peak differential flux reached at this maximal stage of acceleration approached to 10^5 (cm² s sr keV)$^{-1}$ at 50 keV and ~700 (cm² s sr keV)$^{-1}$ at 125 keV.
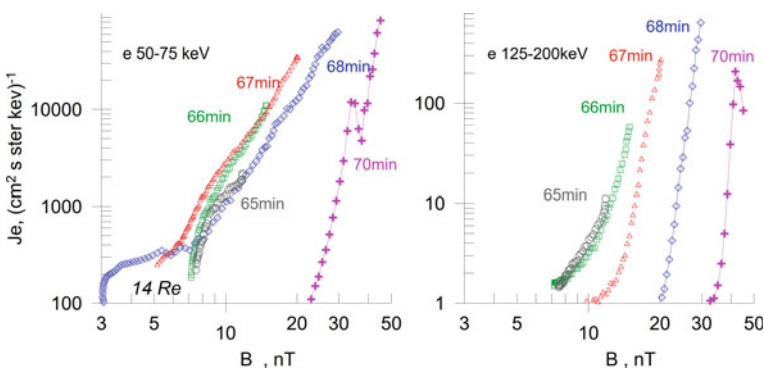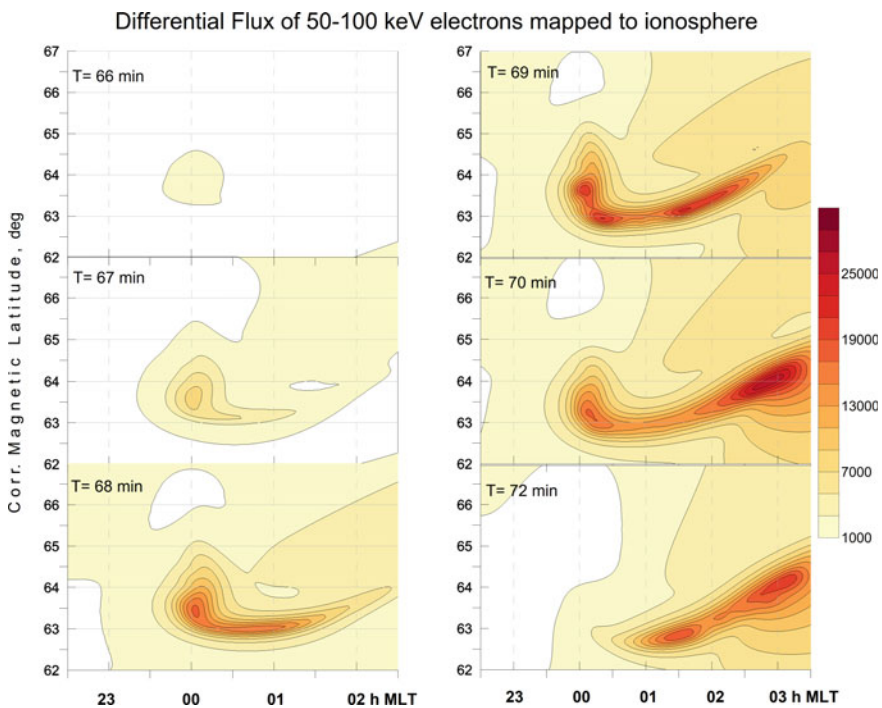

Fig. 3 a Differential flux of 50–75 keV electrons plotted against the magnetic field along the bubble axis (starting from X = −14 Re at the low end and ending where the B peak was attained) for different times during the flow braking stage. Times and colors are the same as in Fig. 2. **b** The same but for 125–200 keV electrons

2.3 Ionospheric View of Injection and Drifting Electron Cloud

Specific assumption of RCM approach is that pitch-angle isotropy is supported for each subpopulation, which automatically provides us with the value of precipitated flux and allows to describe the ionospheric picture of injection-related precipitation which is presented in Fig. 4. As seen in Fig. 3, the energetic particle fluxes are pretty low while the bubble propagates in the plasma sheet (at |X|>10 Re, T < 66 min), therefore equatorial propagation of precipitation at initial stage is not really seen by existing ground-based instruments. Instead, the EE fluxes grow explosively by a factor of 20 between T = 66 and 68 min (centered at the latitude 63.5–64°). The release of injected electrons to azimuthal drift orbits occurs immediately and at 68 min we already see the intense EE precipitation arc on equatorial side extended by ~2 h MLT east, which later quickly expands toward dawn- then noon sectors (Fig. 5).

Spatial dynamics of the injection-related EE precipitation in Fig. 4 is fully consistent with available observations. Particularly, authors of [14] reported that cosmic noise absorption (CNA), observed in the region conjugate to dispersionless injection observed at near-geostationary orbit in the magnetosphere, grows explosively (within

Fig. 4 A sequence of differential flux distributions of 50–75 keV electrons precipitated into the ionosphere during the phase of flow braking and energetic electron injection
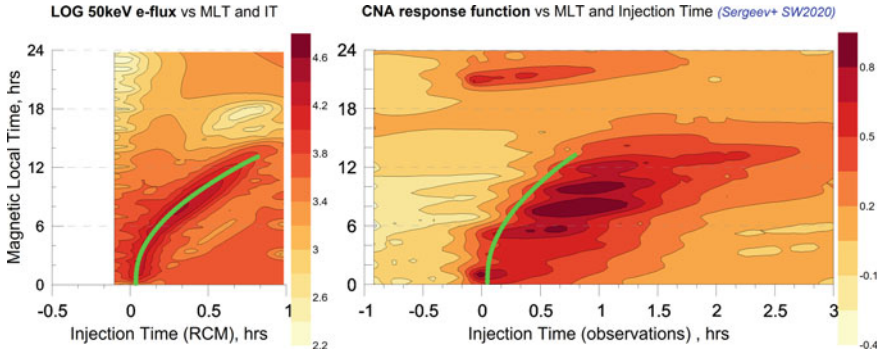
Fig. 5 *Left panel*—Variation of MLT distribution of the peak differential flux of 50–75 keV electrons versus injection time in our simulation; *right panel*–EE precipitation reconstructed from CNA observations in the center of auroral zone in [16]

3 min), whereas the rise time of precipitation is slower for observations conjugate to energy-dispersed electron cloud. Also, spatial scales of injection region (roughly 1° latitude and ~1 h MLT) in Fig. 4 are consistent with the CNA onset observations by imaging riometers reported by [15].

To characterize the azimuthal dynamics of precipitation during an hour following the bubble launch, at each time after injection (injection time, with IT = 0 supposed to be at 67 min) and for each MLT meridian we determined the largest 50 keV flux value and then plotted these values in MLT-IT coordinates. Figure 5 (left panel) shows the eastward drift of compact electron cloud whose speed was fast during first 10 min (when the EE cloud drifted over the nightside magnetotail where the radial B-gradient is larger than on the dayside) and decreased during the passage over the dayside magnetosphere. Green dotted line illustrates the trajectory of EE peak region, it is copied onto the IT-MLT dynamical pattern of EE precipitation reconstructed from CNA observations in the center of auroral zone during 220 substorms in [16]. Indeed, the green line reproduces well the observed dynamics of frontside part of the precipitation region. The longer duration observed in the precipitation is not surprising taking into account that EE cloud in our simulation was formed by the very brief pulse of fast flow whereas during real substorms it is influenced by many activations distributed over the hour timescale.

Comparison of left and right panels shows some more global scale similarities. In both cases the peak precipitation strength occurs at around 8 h MLT and precipitation intensity is significantly depressed while the cloud drifts over the dayside, with the wide precipitation minimum formed in the afternoon-dusk sector. Such crescent-like global distribution with prenoon maximum is a long-known feature of the CNA global distribution (see, e.g., [17]). In simulations there are two reasons for such spatial variation of the drifting cloud. One of them is the acceleration/deceleration of drifting electrons by large-scale convection electric field, which should form the 50 keV flux intensity maximum near dawn and pronounced flux depression near dusk. On the other hand, the precipitation losses from the drifting cloud (included

in this model version) will assist by decreasing the intensity of the cloud drifting eastward from dawn to dusk. Actual role played by each of two physical effects will be quantitatively investigated in the following study.

3 Summary

Our analyses extend previous attempts to simulate the energetic electron injections (e.g., [5, 8–10], etc.) by using fully self-consistent 3D RCM simulation, which starts from realistic configuration, includes particles of different energies and take into account explicitly their magnetic and ExB drifts. Comparing to previous RCM bubble simulation [7], this simulation uses advanced model including inertia effects [11] and it is significantly improved in terms of both spatio-temporal and energy resolution. Here we focus on describing how/where the EE cloud grows and releases; how/where the EE cloud inner boundary is formed, and what is the global dynamics of electrons injected and precipitated into the ionosphere after injection. We confirm previous results that, initiated by the plasma evacuation from the localized plasma tube at 18Re, rapid development of the plasma bubble leads to remarkable energetic electron injection into the inner magnetosphere. Starting from realistic setup, during the bubble propagation the betatron-like acceleration increases their fluxes considerably (by 2–3 orders of magnitude), and most of this increase occurs during a couple of minutes of fast flow braking in the inner magnetosphere. At this time, the 50 keV electron flux can finally achieve as high flux value as 10^5 (cm^2 s sr keV)$^{-1}$, which is typical for substorm-related EE injections observed at the geostationary orbit (e.g., [18]).

During the flow braking phase, it was somewhat unexpected to observe that electrons of different energies (50–200 keV) were transported to the common earthward boundary (injection boundary), which in our case corresponded to the narrow region of strong magnetic gradients in front of the dipolarization front, where energetic electrons were suddenly deflected azimuthally to form the injection boundary. It is interesting that the leading bubble front still continued its inward motion after T = 68 min, so that EE injection boundary and bubble front became dynamically decoupled at later time.

Whereas previous simulations were focused on the injection process itself, for the first time we also described quantitatively the following global dynamics of electrons injected and precipitated into the ionosphere. Particularly we paid attention to sudden growth of precipitation (in a couple of minutes) in a localized region caused by injection, whose time- and spatial scales nicely agree with available observations. When simulating the following propagation of the injected electron cloud, our results demonstrate a good agreement with the dynamics of precipitation front propagation. Also, our simulation is capable to reproduce basic known global features of precipitation pattern including the prenoon precipitation maximum and a crescent-shaped precipitation zone with minimal precipitation at dusk.

References

1. Lezniak, T., and Winckler, J., Experimental study of magnetospheric motions and the acceleration of energetic electrons during substorms, J. Geophys. Res., 75(34), 7075–7098 (1970)
2. Parks, G., The acceleration and precipitation of Van Allen outer zone energetic electrons. J. Geophys. Res., 75(19), 3802–3816 (1970)
3. Rozanov, E., Calisto, M., Egorova et al. Influence of the precipitating energetic particles on atmospheric chemistry and climate. Surveys in Geophysics, 33(3–4), 483–501 (2012)
4. Angelopoulos, V., Baumjohann, W., Kennel, C. et al., Bursty bulk flows in the inner central plasma sheet, J. Geophys. Res., 97(A4), 4027–4039 (1992)
5. Gabrielse, C., Angelopoulos V., Harris C. et al., Extensive electron transport and energization via multiple, localized dipolarizing flux bundles, J. Geophys. Res. Space Physics, 122, 5059–5076 (2017)
6. Chen, C. X., and Wolf, R. A., Interpretation of high-speed flows in the plasma sheet, *J. Geophys. Res.*, 98(A12), 21409–21419 (1993)
7. Yang, J., Toffoletto, F., Wolf, R., and Sazykin, S., RCM-E simulation of ion acceleration during an idealized plasma sheet bubble injection, J. Geophys. Res. Space Physics, 116, A05207 (2011)
8. Birn, J., Hesse, M., Nakamura, R., & Zaharia, S., Particle acceleration in dipolarization events. J. Geophys. Res. Space Physics, 118, 1960–1971 (2013)
9. Li, X., Baker, D., Temerin, M., Reeves, G., & Belian, R., Simulation of dispersionless injections and drift echoes of energetic electrons associated with substorms. Geophys. Res. Lett., 25(20), 3763–3766 (1998)
10. Eshetu, W., Lyon, J., Hudson, M., & Wiltberger, M., Simulations of electron energization and injection by BBFs using high-resolution LFM MHD fields. J. Geophys. Res. Space Physics, 124, 1222–1238 (2019)
11. Yang, J., Wolf, R., Toffoletto, F., et al., The Inertialized Rice Convection Model, J. Geophys. Res. Space Physics, 124, 10294–10317 (2019)
12. Silin, I., Toffoletto, F., Wolf, R., & Sazykin, S. Y., Calculation of magnetospheric equilibria and evolution of plasma bubbles with a new finite-volume MHD/magnetofriction code. American Geophysical Union, Fall Meeting 2013, SM51B-2176 (2013)
13. Sergeev, V. A., Sun, W., Yang, J., & Panov, E. V., Manifestations of magnetotail flow channels in energetic particle signatures at low-altitude orbit. Geophys. Res. Lett., 48, e2021GL093543 (2021)
14. Spanswick, E., Donovan, E., Friedel, R. and Korth, A., Ground based identification of dispersionless electron injections, Geophys. Res. Lett., 34, L03101 (2007)
15. Kellerman, A., and Makarevich R., The response of auroral absorption to substorm onset: Superposed epoch and propagation analyses, J. Geophys. Res. Space Physics, 116, A05312, (2011)
16. Sergeev, V. A., Shukhtina, M. A., Stepanov N. et al., Toward the reconstruction of substorm-related dynamical pattern of the radiowave auroral absorption. Space Weather, 18, e2019SW002385, (2020)
17. Berkey, F. T., Driatskiy, V. M., Henriksen, K., et al., A synoptic investigation of particle precipitation dynamics for 60 substorms in IQSY (1964–1965) and IASY (1969). Planet. Space Sci., 22(2), 255–307 (1974)

18. Nagai, T., Shinohara, I., Singer, H. J., Rodriguez, J., & Onsager, T. G., Proton and electron injection path at geosynchronous altitude. J. Geophys. Res. Space Physics, 124, 4083–4103 (2019)